

A combined level set/ghost cell immersed boundary representation for floating body simulations

Hans Bihs* and Arun Kamath

Department of Civil and Transport Engineering, Norwegian University of Science and Technology (NTNU), 7491 Trondheim, Norway

International Journal For Numerical Methods In Fluids, 2017, **83** (12), pp. 905-916.
DOI: <http://dx.doi.org/10.1002/flid.4333>

Abstract

A six degrees of freedom (6DOF) algorithm is implemented in the open-source CFD code REEF3D. The model solves the incompressible Navier-Stokes equations. Complex free surface dynamics are modeled with the level set method based on a two-phase flow approach. The convection terms of the velocities and the level set method are treated with a high-order WENO discretization scheme. Together with the level set method for the free surface capturing, this algorithm can model the movement of rigid floating bodies and their interaction with the fluid. The 6DOF algorithm is implemented on a fixed grid. The solid-fluid interface is represented with a combination of the level set method and ghost cell immersed boundary method. As a result, re-meshing or overset grids are not necessary. The capability, accuracy and numerical stability of the new algorithm is shown through benchmark applications for the fluid-body interaction problem.

Keywords: 6DOF; floating; level set method; immersed boundary; Computational Fluid Dynamics; REEF3D

1 Introduction

Coupled fluid-structure interaction plays a major role in many engineering disciplines. In the fields of coastal, ocean and arctic engineering, fluid-structure interaction problems occur in the presence of a free water surface and result in complex floating body dynamics. Some examples are floating piers, floating oil platforms, ship motion prediction or floating ice floes. Advanced solutions for the hydrodynamics, which include more complex free surface phenomena such as wave breaking or water jets and viscous effects from turbulence, require the solution of

*Corresponding author, hans.bihs@ntnu.no

Postprint, published in International Journal For Numerical Methods In Fluids, doi: <http://dx.doi.org/10.1002/flid.4333>

the Navier-Stokes equations. In earlier studies, fluid-structure interaction problems based on the Navier-Stokes equations have been calculated with Arbitrary Lagrangian-Eulerian (ALE) methods (Ramaswamy et al. (1986), Walhorn et al. (2005)). Then the interface location between the solid and the fluid is tied to the numerical mesh. When the location of this interface changes, the numerical mesh needs to be adjusted in order to account for this. The re-meshing procedure can have a detrimental effect on the numerical accuracy and stability, especially for more arbitrary solid body movements. Also, for free surface flows, this method can become prohibitively complex.

A way to avoid constant re-meshing is the usage of dynamic overset grids. The method consists of a base mesh, which covers the full flow domain. The overset mesh is placed in the vicinity of the solid structures and overlaps with the base mesh. Then the overset mesh follows the movement of the solid. Carrica et al. (2007) presented a complete framework for the modeling of ship motion using dynamic overset grids. The free surface was treated with a single-phase level set method. The dynamic overset mesh approach has numerical stability advantages over ALE, as constant re-meshing of the solution domain is not necessary. The challenge of the method lies in an accurate, yet stable scheme for establishing the connections between the overset mesh points and the underlying grid points in the overlapping region. Later, Yang and Stern (2009) showed an extension of the dynamic overset mesh approach, where the solid-fluid interface was treated with a sharp interface method instead of overset grids. The free surface was treated with a two-phase level set method. A further iteration of the dynamic overset mesh approach featured a direct forcing immersed boundary method for the fluid-solid interface Yang and Stern (2012). Special attention was given to the field extension method, which was earlier presented for one-phase fluid-structure interaction Yang and Balaras (2006). When the solid moves through the flow field, solid cells becomes fluid cells and vice versa. With the field extension, unphysical values for the pressure and the velocities are avoided, through interpolation and keeping the physical pressure gradients intact. More recently, Calderer et al. (2014) presented a level set based two-phase flow solver for the simulation of floating structures. A curvilinear immersed boundary method was used for the fluid-solid interface Borazjani et al. (2008). Chen et al. (2016) presented a strong, two-way, fluid-solid coupling algorithm, based on a variational-type cut cell methodology, implemented within a hybrid Eulerian-Lagrangian framework.

Smoothed Particle Hydrodynamics (SPH) methods have also been used to calculate fluid-floating structure interaction by Bouscasse et al. (2013) using a ghost fluid method to enforce the solid-fluid boundary for two-dimensional problems. Omidvar et al. (2013) used an SPH implementation for 3D floating bodies using variable mass distribution to make the model computationally efficient. A large number of particles are required to accurately simulate the hydrodynamics of floating bodies using these methods. Glowinski et al. (2001) presented a Lagrange multiplier based fictitious domain decomposition method for the simulation of an airfoil and sedimentation of circular particles. Sueyoshi et al. (2008) simulated wave induced nonlinear motions of a two-dimensional box-shaped floating body using a moving particle semi-implicit (MPS) method but had difficulties with shorter period waves in sway and heave motions and a phase shift in the wave elevation.

In the present manuscript the open-source CFD code REEF3D is used. The model has been used extensively for complex wave hydrodynamics problems in the field of coastal and ocean engineering such as breaking waves Alagan Chella et al. (2015) Alagan Chella et al. (2015), wave energy converter devices Kamath et al. (2015*b*), non-breaking wave forces Ka-

math et al. (2015a) and breaking wave forces Bihs et al. (2016). A novel approach for the geometry description for the 6DOF (six degree of freedom) algorithm is proposed. With the combined use of triangular surface meshes and the level set method, the fluid force and momentum can be integrated in a straightforward manner. The solid body is immersed into the fluid and re-meshing or overset grids are avoided. This is achieved with the local directional immersed boundary (Berthelsen and Faltinsen, 2008) in this study. The presented results are all obtained with a weakly coupled scheme. In combination with an already robust two-phase flow solver, this results in a stable fluid-structure interaction model. Numerical results for a disc entry problem, a free falling wedge and roll decay and roll motion of a rectangular barge under the influence of waves are presented.

2 Numerical Model

The governing equations of the numerical model are the continuity and the incompressible Navier-Stokes (NS) equations presented in compact tensor notation:

$$\frac{\partial u_i}{\partial x_i} = 0 \quad (1)$$

$$\frac{\partial u_i}{\partial t} + u_j \frac{\partial u_i}{\partial x_j} = -\frac{1}{\rho} \frac{\partial p}{\partial x_i} + \frac{\partial}{\partial x_j} \left[\nu \left(\frac{\partial u_i}{\partial x_j} + \frac{\partial u_j}{\partial x_i} \right) \right] + g_i \quad (2)$$

where u is the velocity averaged over time t , ρ is the fluid density, p is the pressure, ν is the kinematic viscosity and g the acceleration due to gravity.

A Cartesian grid is used to discretize the spatial domain, providing easy implementation of higher-order discretization schemes. The model employs a staggered numerical grid to ensure better pressure-velocity coupling and avoid numerical instabilities. The convective terms of the NS equations are discretized with a fifth-order WENO (weighted essentially non-oscillatory) scheme by Jiang and Shu Jiang and Shu (1996) in the conservative finite-difference framework. The conservative WENO scheme is used to treat the convective terms for the velocities u_i , while a Hamilton-Jacobi version Jiang and Peng (2000) is used for the variables of the free surface algorithm. The Hamilton-Jacobi version approximates the spatial derivatives at integer grid points rather than at half-integer points in the conservative version and is more suitable for the approximation of the gradients in the level set function.

For the time treatment a second-order accurate TVD Runge-Kutta scheme is employed, solving the Poisson equation two times per full time-step consisting of two Euler steps Shu and Osher (1988):

$$\begin{aligned} \Phi^{(1)} &= \Phi^n + \Delta t L(\Phi^n) \\ \Phi^{(n+1)} &= \frac{1}{2} \Phi^n + \frac{1}{2} \Phi^{(1)} + \frac{1}{2} \Delta t L(\Phi^{(1)}) \end{aligned} \quad (3)$$

Adaptive time stepping is used in order to control the time steps and ensure numerical stability by maintaining the required CFL number. Chorin's projection method for incompressible flow which is first-order accurate, is used for the treatment of the pressure Chorin (1968). During the solution of the NS equations at each Euler step of the Runge-Kutta time stepping procedure, the pressure gradient is excluded. Based on the resulting divergence of

the flow, a Poisson equation for the pressure is formed with the right hand side containing the continuity defect $\frac{\partial u_i^*}{\partial x_i}$ in Eq. 4, where u_i^* is the transient velocity. The Poisson equation is solved using the fully parallelized Jacobi-preconditioned BiCGStab algorithm van der Vorst (1992). The gradient of the new pressure field is then used to correct the velocity field, making it divergence free.

$$-\frac{\partial}{\partial x_i} \left(\frac{1}{\rho(\Phi^{n+1})} \frac{\partial p}{\partial x_i} \right) = -\frac{1}{\Delta t} \frac{\partial u_i^*}{\partial x_i} \quad (4)$$

The location of the free water surface is represented implicitly by the zero level set of the smooth signed distance function $\Phi(\vec{x}, t)$ Osher and Sethian (1988). The level set function gives the closest distance to the interface and the two phases are distinguished by the change of the sign. This results in the following properties:

$$\Phi(\vec{x}, t) \begin{cases} > 0 \text{ if } \vec{x} \in \text{phase 1} \\ = 0 \text{ if } \vec{x} \in \Gamma \\ < 0 \text{ if } \vec{x} \in \text{phase 2} \end{cases} \quad (5)$$

In addition, the Eikonal equation $|\nabla\phi| = 1$ is valid. When the interface Γ is moved under an externally generated velocity field \vec{v} , a convection equation for the level set function is obtained:

$$\frac{\partial \Phi}{\partial t} + u_j \frac{\partial \Phi}{\partial x_j} = 0 \quad (6)$$

When the interface evolves, the level set function loses its signed distance property. In order to maintain this property and to ensure mass conservation, the level set function is initialized after each time step. In the present paper a PDE based reinitialization equation is solved Sussman et al. (1994):

$$\frac{\partial \Phi}{\partial t_p} + S(\Phi) (|\nabla\Phi| - 1) = 0 \quad (7)$$

where t_p is psuedo time and $S(\Phi)$ is the smoothed sign function Peng et al. (1999). The material properties of the two phases can be then be determined for the whole domain. Close to the interface, the density ρ and the viscosity ν are smoothed out by calculating the density at the cell face with a regularized Heaviside function with an interface thickness of $\epsilon = 2.1dx$:

$$\rho_{i+\frac{1}{2}} = \rho_1 H\left(\Phi_{i+\frac{1}{2}}\right) + \rho_2 \left(1 - H\left(\Phi_{i+\frac{1}{2}}\right)\right) \quad (8)$$

The level set function at the cell face is obtained using:

$$\Phi_{i+\frac{1}{2}} = \frac{1}{2} (\Phi_i + \Phi_{i+1}) \quad (9)$$

3 6DOF Algorithm

For the calculation of fluid-structure interaction, the geometry of the solid body needs to be defined. In the current model, it is described by a primitive triangular surface mesh neglecting

connectivity. By design, this resembles the structure of the STL format, a standard for surface meshes, available in most CAD and meshing softwares (Chua and Leong, 2003).

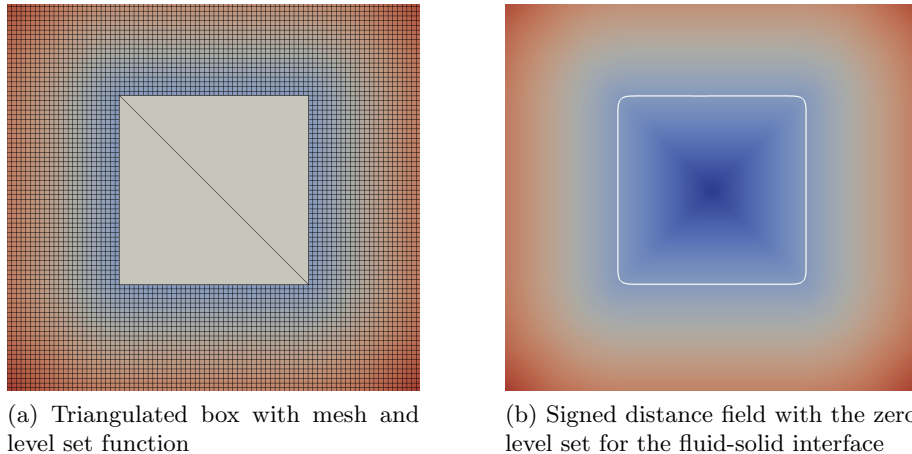


Figure 1: Representation of the solid body with a level set function.

The intersections of the surface mesh with the underlying Cartesian grid are determined with a ray-tracing algorithm (Yang and Stern, 2013). Here, inside-outside information and the shortest distance to the closest triangle for the grid points along the coordinate axis can be calculated in a very efficient and reliable manner. After this step, the standard reinitialization algorithm Peng et al. (1999) is used to get signed distance properties for the level set function in the vicinity of the solid body, see Fig. 1. In current literature, the level set method has been employed to represent moving solid bodies by Cheny and Botella (2010) and Baiges et al. (2011). It is important to mention, that the ray-tracing algorithm calculates the distances in an exact manner close to the solid boundary, which results in a sharp representation of the solid-fluid interface. The moving solid-fluid interface is treated with the ghost cell immersed boundary method Berthelsen and Faltinsen (2008). The forces acting on the surface Ω of the floating body can be determined for each co-ordinate direction i separately using the pressure p and the viscous stress tensor τ in the following way:

$$F_{i,e} = \int_{\Omega} (-\mathbf{n}_i p + \mathbf{n}_i \cdot \tau) d\Omega \quad (10)$$

The distance of the center of gravity from the origin of the body-fitted grid can be determined using the following equation 11:

$$\mathbf{r}_{cg} = \frac{1}{m} \int_V \mathbf{r} \rho_a dV \quad (11)$$

where \mathbf{r} is the distance from each surface cell to the origin of the body-fitted co-ordinate system. Assuming that the origin of the body-fitted co-ordinate system is at the center of gravity of the floating body, \mathbf{r} is the distance of each surface cell to the center of gravity and the moments are determined as follows:

$$L_{i,e} = \int_{\Omega} \mathbf{r} \times (-\mathbf{n}_i p + \mathbf{n}_i \cdot \tau) d\Omega \quad (12)$$

where

$$\begin{aligned}
 [m(\dot{u} - vr + wq)] &= X \\
 [m(\dot{v} - wp + ur)] &= Y \\
 [m(\dot{w} - uq + vp)] &= Z \\
 [I_x \dot{p} + (I_z - I_y)qr] &= K \\
 [I_y \dot{q} + (I_x - I_z)rp] &= M \\
 [I_z \dot{r} + (I_y - I_x)pq] &= N
 \end{aligned} \tag{18}$$

Here u, v, w, p, q and r are the values for the linear and angular velocities from the previous time step. Then $\dot{u}, \dot{v}, \dot{w}, \dot{p}, \dot{q}$ and \dot{r} can be calculated in an explicit manner. Any of the linear and angular velocities $\dot{\varphi}$ and any component of the position and orientation vector φ of the floating body can be calculated with a second-order Adams-Bashforth scheme for the new time step:

$$\begin{aligned}
 \dot{\varphi}^{n+1} &= \dot{\varphi}^n + \frac{\Delta t}{2} (3\ddot{\varphi}^{n+1} - \ddot{\varphi}^n) \\
 \varphi^{n+1} &= \varphi^n + \frac{\Delta t}{2} (3\dot{\varphi}^{n+1} - \dot{\varphi}^n)
 \end{aligned} \tag{19}$$

As a result, the floating body dynamics are solved in a fully explicit way. Even though the weak coupling between the 6DOF algorithm and the flow solver has been reported to lead to numerical stability problems for complex cases (e.g. Carrica et al. (2007) or Calderer et al. (2014)), the current implementation shows good numerical stability throughout the range of applications.

The dynamic rigid body equations have been solved in the floating body reference frame. The translations and orientations are also calculated there. They are transformed to the inertial reference frame with the matrix given in Eq. 16. The angular velocities are transformed using the following rotation matrix \mathbf{J}_2 (Fossen, 1994) where s , c and t stand for *sin*, *cos* and *tan* respectively:

$$\dot{\boldsymbol{\eta}}_2 = \begin{bmatrix} 1 & s\phi & t\theta & c\phi & t\theta \\ 0 & c\phi & -s\phi & & \\ 0 & s\phi/c\theta & c\phi/c\theta & & \end{bmatrix} \mathbf{v}_2 = \mathbf{J}_2 \mathbf{v}_2 \tag{20}$$

Boundary conditions for the velocities on the solid-fluid interface result from the motion of the solid body with respect to its center of gravity.

$$\mathbf{u}_i = \dot{\boldsymbol{\eta}}_1 + \dot{\boldsymbol{\eta}}_2 \times \mathbf{r} \tag{21}$$

Pressure oscillations in the vicinity of the solid body can occur due to solid cells turning into fluid cells and vice versa. This is avoided by the implementing the field extension method Udaykumar et al. (2001) Yang and Balaras (2006) adapted to the ghost cell immersed boundary method. For non-moving boundaries, a zero-gradient boundary condition is used for the

pressure. In order to maintain a physical pressure gradient near the floating body, the following boundary condition for the gradient of the pressure is given:

$$\frac{\partial p}{\partial x_i} = -\frac{1}{\rho} \frac{Du_i}{Dt} \quad (22)$$

In order to determine u_i , one possibility is to evaluate the momentum equations. A simpler way is to differentiate Eq. 21 with respect to time and use this for the ghost cell values for the pressure:

$$\frac{Du_i}{Dt} = \frac{d}{dt} (\dot{\boldsymbol{\eta}}_1 + \dot{\boldsymbol{\eta}}_2 \times \mathbf{r}) \quad (23)$$

When cells are freshly cleared by the moving body and become fluid cells, unphysical values for the velocities and the pressure in those cells can cause numerical stability problems. This is avoided by assigning the velocities the values from Eq. 21 and the value for the pressure is found through interpolation from the fluid.

4 Results

4.1 Disc Entry

At first the 6DOF algorithm is tested for the well-known disc entry problem. This case has been used by several authors to benchmark their models (e.g. Yang and Stern (2009) or Calderer et al. (2014)). The parameters for the geometry, the initial boundary conditions and flow parameters of this test are non-dimensional. The disc enters the water with the fixed vertical velocity of $V = -1$. The center of the disc is located at $H = 1.25$ over the free surface at $T = Vt/H = 0$. The cylinder has a radius of $R = 1$. The two-dimensional simulation domain has the size $30R \times 22R$. The uniform mesh size is $dx = 0.025$, resulting in 1200×880 grid cells. Acceleration due to gravity is $g = -1$, the density of the water is $\rho_{water} = 1$, the density of the air is $\rho_{air} = 0.001$, the viscosity of the water is $\nu_{water} = 0.001$ and the viscosity of the air is $\nu_{air} = 0.018$. The time step size is controlled with adaptive time stepping using a CFL number of 0.1. No turbulence model is employed for this case.

The free surface location and contour for the velocity magnitude are shown in Fig. 2. The disc enters the liquid phase in Fig. 2a. In a symmetric fashion, breaking waves are generated from the solid impact at the sides of the disc and are traveling away from the disc. A fine enough mesh is necessary for capturing breaking waves, in general terms Alagan Chella et al. (2015), but also specifically for the present case Calderer et al. (2014). In Fig. 2b, the post-breaking waves are moving further away towards the side boundaries. At $T = 3.0$, the displaced water has started to return to the location of the disc impact, and the solid body is now fully submerged in the liquid phase. At $T = 4.0$, the returning water creates a vertical water jet. The free surface location compares well with other results reported in literature (e.g. Yang and Stern (2009) or Calderer et al. (2014)).

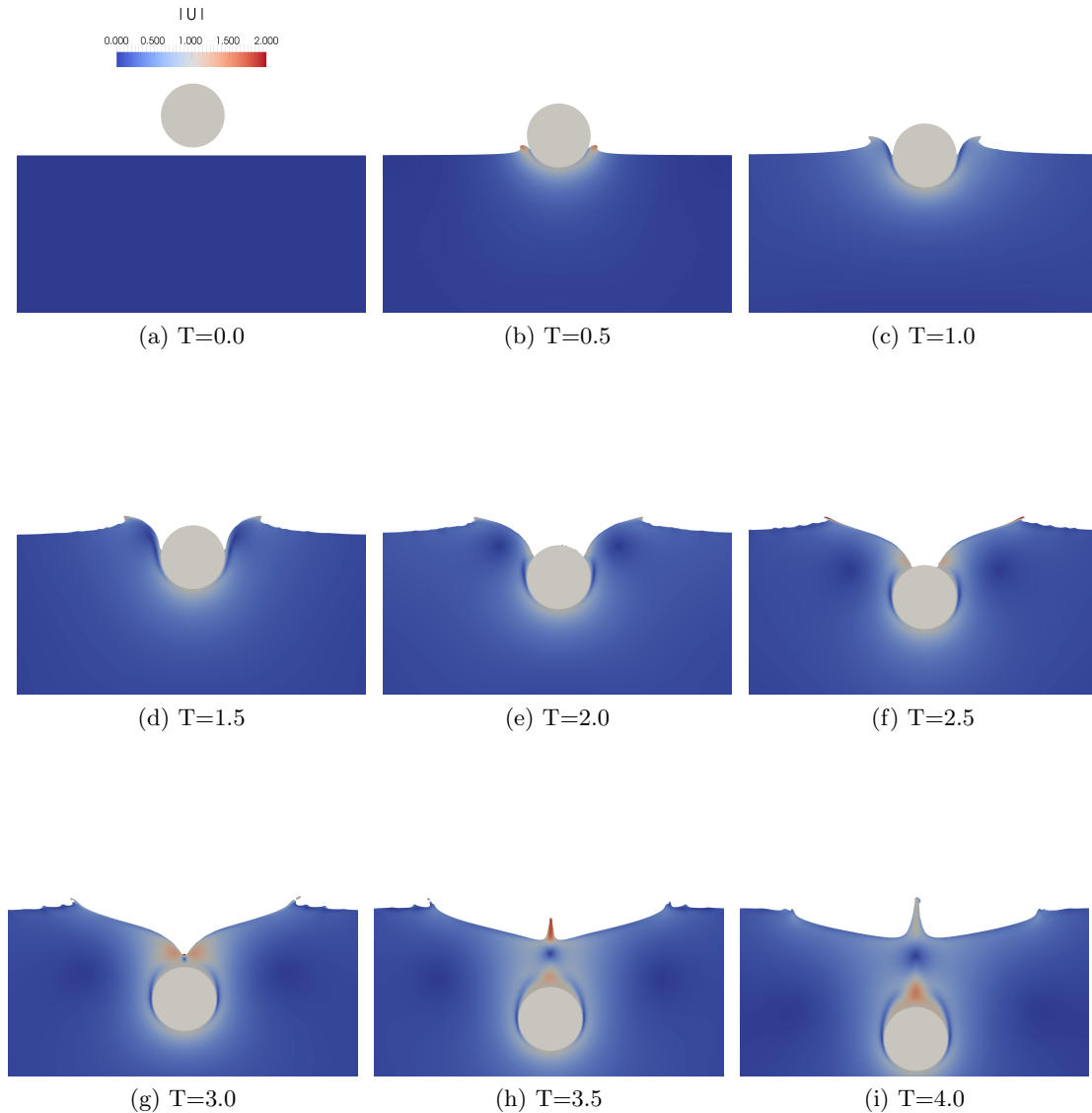


Figure 2: Disc entry problem, the contour shows the velocity magnitude.

4.2 Free Falling Wedge

In the previous section, the motion of the solid body was fixed. In this section, the free falling wedge has all degrees of freedom in the two-dimensional plane. The numerical setup is similar to the experiments by Yettou et al. (2006). The solid wedge has a density of $\rho = 466.6 \text{ kg/m}^3$. The bottom sides have an angle of 25° with respect to the x-axis and the wedge is 1.2 m wide. The time step size is controlled with adaptive time stepping using a CFL number of 0.1. As this case evolves rapidly over a span of only a few seconds, no turbulence model is used.

The distance from the tip of the wedge to the free surface is 1.3 m in the initial stage of the experiment. The water depth is 1 m. In the experiments, the wedge was released into a 27 m long tank. In the present simulations the length of the tank is 8 m. As a result,

some amount of reflections from the side walls can be expected, while they are negligible in the experiments. The numerical results are shown in Fig. 3. The wedge is released at $t = 0.0$ s and then accelerates downwards driven by gravity. At $t = 0.5$ s, the wedge is close to impact with the free surface. The contour shows the velocity magnitude. From this it can be seen that at $t = 0.5$ s, the velocity is maximum just after impact. From the impact, the displaced water rapidly moves away from the wedge in the form of two symmetric waves (Fig. 3e), which are breaking at $t = 0.8$ s. Then, the waves are reflected by the side walls at $t = 1.35$ s. Because the wedge is significantly lighter than the water, the body does not get fully submerged. Instead, it is floating and moving up and down with the reflected waves.

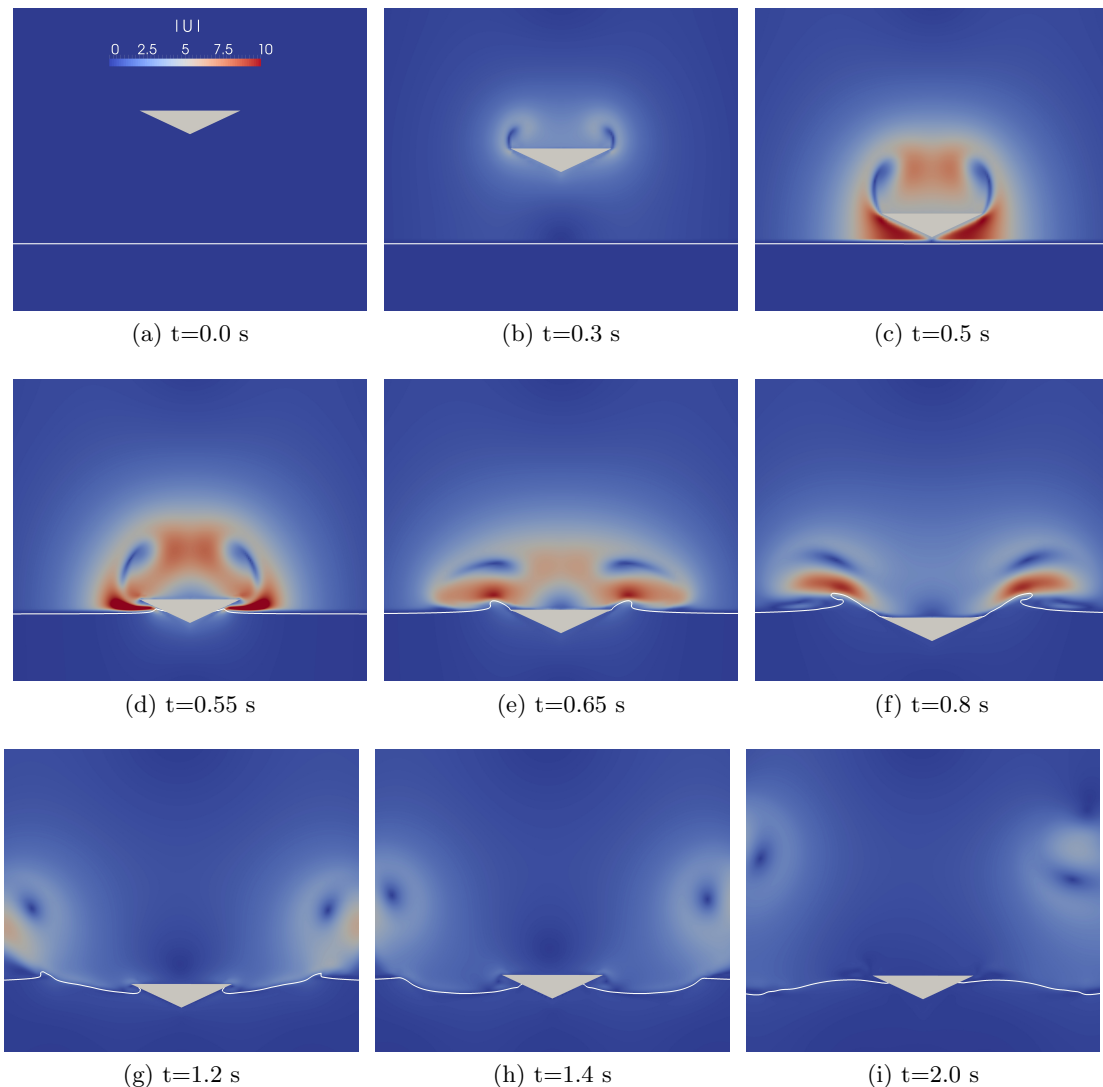


Figure 3: Free falling wedge, the contour shows the velocity magnitude.

Fig. 4a shows the vertical position of the center of gravity of the wedge, which is measured from the still water level. In the first 0.5 s of the free fall, the wedge moves downwards and hits the free surface, which can also be seen in Fig. 3d. Then the wedge moves into the body

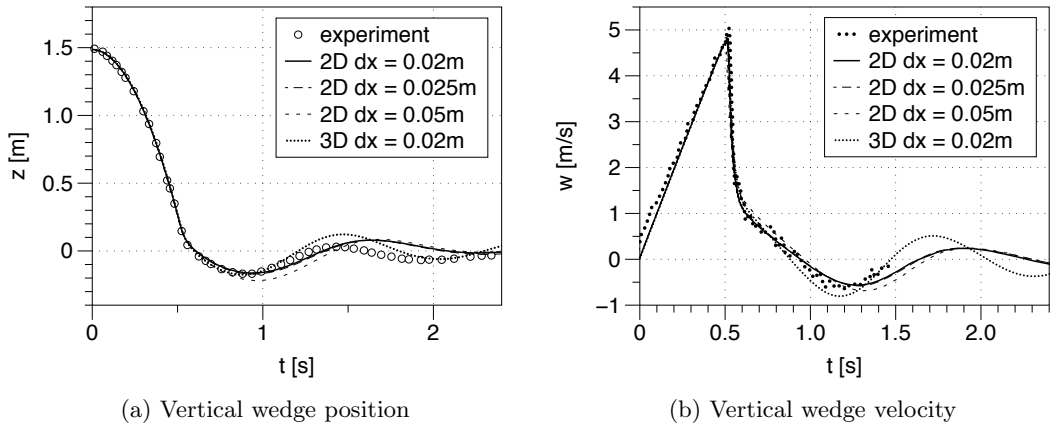


Figure 4: Motion of a wedge under free-fall

of water and starts to oscillate around the still water level. Three different grid sizes are tested in 2D and one simulation is carried out in 3D. The result for the two finest grids are almost similar in 2D and comparable to the results in 3D. A marginal difference can be found for the grid with $dx = 0.05$ m. Here, the wedge moves slightly deeper into the water after the impact than in the experiments and the fine grid results. The vertical velocity of the wedge is shown in Fig. 4b. In the free fall phase, the velocity is increasing linearly under acceleration due to gravity. After it reaches the peak velocity of 5.5 m/s, the wedge sharply decelerates due to the water impact. When the wedge starts to oscillate around the still water level, the vertical velocity becomes non-linear. The vertical velocity is modeled accurately on all three grids, with slight deviations on $dx = 0.05$ m.

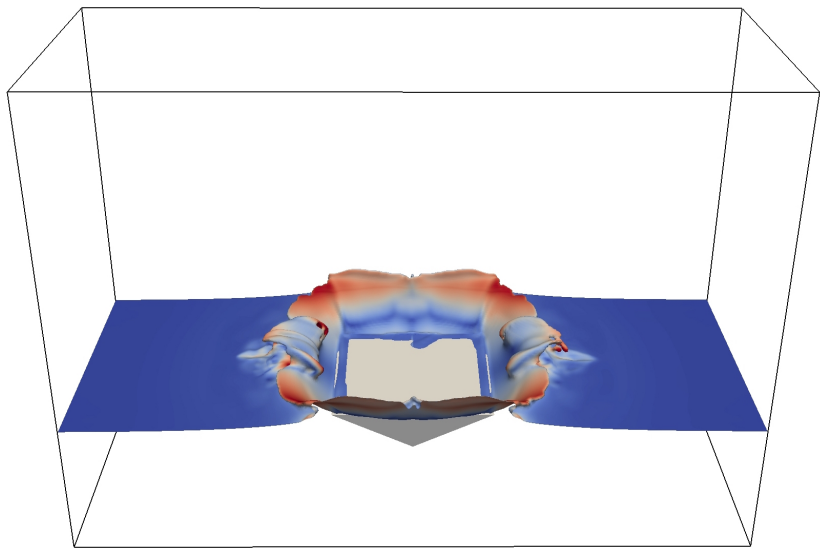


Figure 5: 3D simulation of free falling wedge into water at $t = 0.8$ s

4.3 Roll motion of a rectangular barge

The result from the 3D simulation during water entry of the wedge at $t = 0.8$ s is presented in Fig. 5, showing the splash up of the water as the freely falling wedge impacts the free surface. This scenario involves large pressure gradients as the wedge impinges the fluid surface and typically requires strongly coupled schemes to solve the fluid structure interaction problem according to Calderer et al. (2014). In the current study, this complex fluid structure scenario is solved with a weakly coupled scheme with good results.

The case of roll motion of a rectangular barge in waves has been presented by Jung et al. (2006). They performed experiments in a wave flume with the barge fixed around the rotational direction axis in the center of gravity of the structure, resulting in a single degree of freedom. The barge is 0.3 m long, 0.1 m high and 0.9 m wide. It is made of solid acrylic glass with the density $\rho = 1048$ kg/m³, resulting in a moment of inertia $I_y = 0.236$ kg m² for the direction of the roll motion. The wave flume has a water depth of $h = 0.9$ m. The center of gravity of the barge coincides with the still water free surface location.

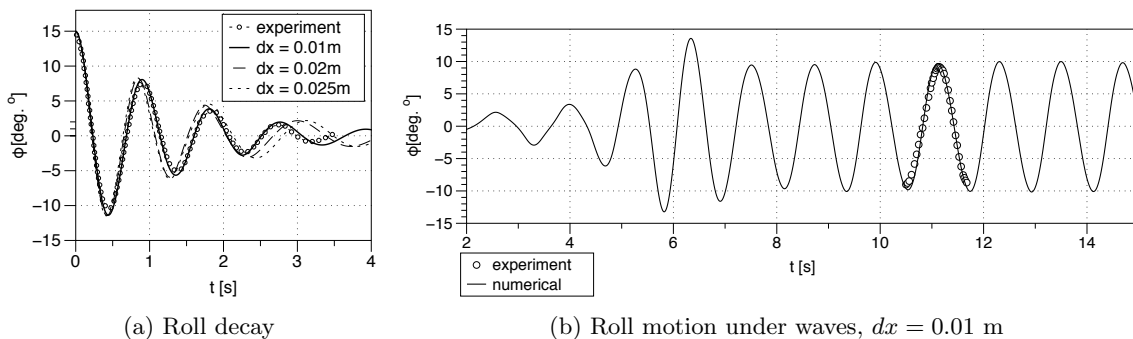


Figure 6: Roll motion of a rectangular barge.

For the roll decay test, the barge is initially tilted to an angle of 15° and then released. In the experiments, the roll angle is recorded with a rotary position sensor. In the numerical simulations the case is treated as two-dimensional, as it is symmetric along the width. The numerical domain for the roll decay test is 5 m long and 1.6 m high, the inflow and outflow boundaries are modeled as walls. A uniform mesh size of $dx = 0.01$ m is used, resulting in a moment of inertia of $I_y = 0.0026$ kg m² for the 0.01 m wide barge. Following Calderer et al. (2014), the damping coefficient of $C = 0.275$ for the three-dimensional case is used in the rigid body equations and adjusted to the two-dimensional setup, in order to account for the friction of the experimental apparatus. No turbulence model is used. Fig. 6a shows the comparison between the experimental and numerical results for the roll decay test. For the acrylic glass barge, the calculated roll angle ϕ for $dx = 0.01$ m agrees well with measurements up to around 3 s. Small differences are observed for the roll decay on the coarser meshes. After that, the numerical results go out of phase.

The roll motion of the rectangular barge under the influence of regular periodic waves is shown in Fig. 6b. Waves with a length of $L = 2.2$ m, a wave period of $T = 1.2$ s and a height $H = 0.06$ m are generated in the numerical model with the relaxation method Jacobsen et al. (2012) Alagan Chella et al. (2015). The simulation domain is $L = 12$ m long, the wave generation zone is 2.2 m long and the numerical beach is 4.4 m long. Fig. 6b shows the

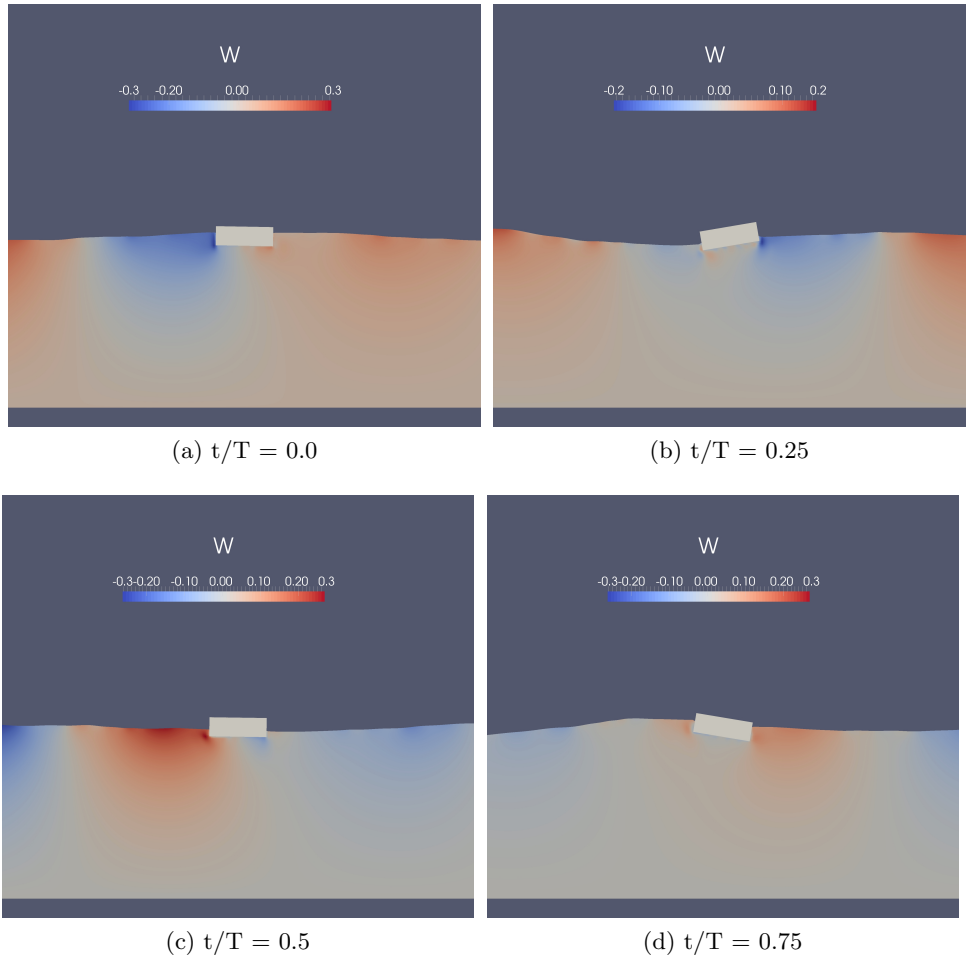


Figure 7: Roll motion of the rectangular barge, the contour shows the vertical velocity.

roll angle. When the first full wave has propagated to the barge from the generation zone, the roll angle shows two maximum peaks in the numerical results. After that, the roll angle maintains a constant amplitude and the measured and computed values from the finest grid show a good match. In Fig. 7, the rectangular barge is shown at different stages of a wave cycle. The contour shows the vertical velocity.

5 Conclusions

The implementation of a 6DOF algorithm in the open-source CFD code REEF3D was shown. In a novel approach, the floating body is represented by the combination of a surface mesh, a level set function and the ghost cell immersed boundary method. This results in a method, that does not require re-meshing or overset grids. The level set method for the description of the surface area of the floating body has the advantage, that the forces and moments can be calculated without explicitly defining the intersections between the surface mesh and the grid of the flow domain. In addition, the numerical model uses the level set method

for the capturing of the interface between water and air. The resulting model proved to be numerically stable and all simulations were performed with a weakly coupled fluid-structure interaction scheme. The three benchmark cases disc entry, free falling wedge and roll motion of a rectangular were calculated successfully and a high level of detail and accuracy was achieved. With the new 6DOF algorithm many interesting problems in coastal, ocean and arctic engineering can be investigated in the future.

Acknowledgements

This study has been carried out under the OWCBW project (No. 217622/E20) and the authors are grateful to the grants provided by the Research Council of Norway.

References

- Alagan Chella, M., Bihs, H. and Myrhaug, D. (2015). Characteristics and profile asymmetry properties of waves breaking over an impermeable submerged reef. *Coastal Engineering*, **100**, 26–36.
- Alagan Chella, M., Bihs, H., Myrhaug, D. and Muskulus, M. (2015). Breaking characteristics and geometric properties of spilling breakers over slopes. *Coastal Engineering*, **95**, 4–19.
- Baiges, J., Codina, R. and Coppola-Owen, H. (2011). The fixed-mesh ALE approach for the numerical simulation of floating solids. *International Journal for Numerical Methods in Fluids*, **67**(8), 1004–1023.
- Berthelsen, P.A. and Faltinsen, O.M. (2008). A local directional ghost cell approach for incompressible viscous flow problems with irregular boundaries. *Journal of Computational Physics*, **227**, 4354–4397.
- Bihs, H., Kamath, A., Alagan Chella, M. and Arntsen, Ø.A. (2016). Breaking-wave interaction with tandem cylinders under different impact scenarios. *Journal of Waterway, Port, Coastal, and Ocean Engineering*. 10.1002/fld.433310.1061/(ASCE)WW.1943-5460.0000343.
- Borazjani, I., Ge, L. and Sotiropoulos, F. (2008). Curvilinear immersed boundary method for simulating fluid structure interaction with complex 3d rigid bodies. *Journal of Computational Physics*, **227**, 7587–7620.
- Bouscasse, B., Colagrossi, A., Marrone, S. and Antuono, M. (2013). Nonlinear water wave interaction with floating bodies in SPH. *Journal of Fluids and Structures*, **42**, 112–129.
- Calderer, A., Kang, S. and Sotiropoulos, F. (2014). Level set immersed boundary method for coupled simulation of air/water interaction with complex floating structures. *Journal of Computational Physics*, **277**, 201–227.
- Carrica, P.M., V., W.R., Noack, R.W. and Stern, F. (2007). Ship motions using single-phase level set with dynamic overset grids. *Computer Fluids*, **36**, 1415–1433.

- Chen, Q., Zang, J., Dimakopoulos, A.S., Kelly, D.M. and Williams, C.J.K. (2016). A cartesian cut cell based two-way strong fluid–solid coupling algorithm for 2d floating bodies. *Journal of Fluids and Structures*, **62**, 252–271.
- Cheny, Y. and Botella, O. (2010). The LS-STAG method: A new immersed boundary/level-set method for the computation of incompressible viscous flows in complex moving geometries with good conservation properties. *Journal of Computational Physics*, **229**(4), 1043–1076.
- Chorin, A. (1968). Numerical solution of the Navier-Stokes equations. *Mathematics of Computation*, **22**, 745–762.
- Chua, C.K. and Leong, K.F. (2003). *Rapid prototyping: principles and applications*, volume 1. World Scientific.
- Fossen, T.I. (1994). *Guidance and Control of Ocean Vehicles*. John Wiley Sons.
- Glowinski, R., Pan, T.W., Hesla, T.I., Joseph, D.D. and Periaux, J. (2001). A fictitious domain approach to the direct numerical simulation of incompressible viscous flow past moving rigid bodies: application to particulate flow. *Journal of Computational Physics*, **169**(2), 363–426.
- Jacobsen, N.G., Fuhrman, D.R. and Fredsøe, J. (2012). A wave generation toolbox for the open-source CFD library: OpenFOAM. *International Journal for Numerical Methods in Fluids*, **70**(9), 1073–1088.
- Jiang, G.S. and Peng, D. (2000). Weighted ENO schemes for Hamilton Jacobi equations. *SIAM Journal of Scientific Computing*, **21**, 2126–2143.
- Jiang, G.S. and Shu, C.W. (1996). Efficient implementation of weighted ENO schemes. *Journal of Computational Physics*, **126**, 202–228.
- Jung, K.H., Chang, K.A. and Jo, H.J. (2006). Viscous effect on the roll motion of a rectangular structure. *Journal of Engineering Mechanics*, **132**(2), 190–200.
- Kamath, A., Alagan Chella, M., Bihs, H. and Arntsen, Ø.A. (2015a). Cfd investigations of wave interaction with a pair of large tandem cylinders. *Ocean Engineering*, **108**, 738–748.
- Kamath, A., Bihs, H. and Arntsen, Ø.A. (2015b). Numerical investigations of the hydrodynamics of an oscillating water column. *accepted to Ocean Engineering*.
- Omidvar, P., Stansby, P.K. and Rogers, B.D. (2013). SPH for 3D floating bodies using variable mass particle distribution. *International Journal for Numerical Methods in Fluids*, **72**(4), 427–452.
- Osher, S. and Sethian, J.A. (1988). Fronts propagating with curvature-dependent speed: Algorithms based on Hamilton-Jacobi formulations. *Journal of Computational Physics*, **79**, 12–49.
- Peng, D., Merriman, B., Osher, S., Zhao, H. and Kang, M. (1999). A PDE-based fast local level set method. *Journal of Computational Physics*, **155**, 410–438.

- Ramaswamy, B., Kawahara, M. and Nakayama, T. (1986). Lagrangian finite element method for the analysis of two-dimensional sloshing problems. *International Journal for Numerical Methods in Fluids*, **6**, 659–670.
- Shu, C.W. and Osher, S. (1988). Efficient implementation of essentially non-oscillatory shock capturing schemes. *Journal of Computational Physics*, **77**, 439–471.
- Sueyoshi, M., Kashiwagi, M. and Naito, S. (2008). Numerical simulation of wave-induced nonlinear motions of a two-dimensional floating body by the moving particle semi-implicit method. *Journal of Marine Science and Technology*, **13**(2), 85–94.
- Sussman, M., Smereka, P. and Osher, S. (1994). A level set approach for computing solutions to incompressible two-phase flow. *Journal of Computational Physics*, **114**, 146–159.
- Udaykumar, H.S., Mittal, R., Rampunggoon, P. and Khanna, A. (2001). A sharp interface cartesian grid method for simulating flows with complex moving boundaries. *Journal of Computational Physics*, **174**, 345–380.
- van der Vorst, H. (1992). BiCGStab: A fast and smoothly converging variant of Bi-CG for the solution of nonsymmetric linear systems. *SIAM Journal of Scientific Computing*, **13**, 631–644.
- Walhorn, E., Kölke, A., Hübner, B. and Dinkler, D. (2005). Fluid–structure coupling within a monolithic model involving free surface flows. *Computer & Structures*, **83**, 2100–2111.
- Yang, J. and Balaras, E. (2006). An embedded-boundary formulation for large-eddy simulation of turbulent flows interacting with moving boundaries. *Journal of Computational Physics*, **215**, 12–40.
- Yang, J. and Stern, F. (2009). Sharp interface immersed-boundary/level-set method for wave–body interactions. *Journal of Computational Physics*, **228**(17), 6590–6616.
- Yang, J. and Stern, F. (2012). A simple and efficient direct forcing immersed boundary framework for fluid–structure interactions. *Journal of Computational Physics*, **231**, 5029–5061.
- Yang, J. and Stern, F. (2013). Robust and efficient setup procedure for complex triangulations in immersed boundary simulations. *Journal of Fluids Engineering*, **135**(10), 101107.1–101107.11.
- Yettou, E.M., Desrochers, Y. and Champoux, Y. (2006). Experimental study on the water impact of a symmetrical wedge. *Fluid Dynamics Research*, **38**, 47–66.